K. Braganza · D.J. Karoly · A.C. Hirst · M.E. Mann
P. Stott · R.J. Stouffer · S.F.B. Tett

Simple indices of global climate variability and change: Part I – variability and correlation structure

Abstract Some simple indices are used to describe global climate variability in observational data and climate model simulations. The indices are surface temperature based and include the global-mean, the land–ocean contrast, the meridional gradient, the inter-hemispheric contrast, and the magnitude of the annual cycle. These indices contain information independent of the variations of the global-mean temperature for un-forced climate variations. They also represent the main features of the modelled surface temperature response to increasing greenhouse gases in the atmosphere. Hence, they should have a coherent response for greenhouse climate change. On interannual and decadal time scales, the variability and correlation structure of the indices from long control climate model simulations compare well with those from detrended instrumental observations for the twentieth century and proxy based climate reconstructions for 1700–1900. The indices provide a simple but effective way to evaluate global-scale climate variability in control climate model simulations. On decadal time scales, the observed correlation structure between the indices during the twentieth century shows significant differences from the detrended observations and control model simulations. These changes are consistent with forced climate variations in greenhouse climate change simulations. This suggests that the changes in the correlation structure between these indices can be used as an indicator of climate change.

1 Introduction

There has been much recent public and scientific interest in climate variability and change, and the possible role of human activity in observed climate change. A comprehensive assessment of scientific understanding of this subject is provided in the IPCC Third Assessment Report (TAR) (Houghton et al. 2001). Several related issues that arise from that assessment are considered in this study. They include evaluation of the performance of climate models in simulating unforced, internal variability of the climate system, comparison of forced climate model simulations with the recent observed climate record, and a simple approach for communicating information about changes in global-scale surface temperature patterns.

Most studies of climate variability and change have considered variations of surface air temperature because it has a reasonably long and high quality observational record. Many studies have used the global-mean surface temperature to establish the degree and significance of changes in climate over the last century. This is because global-mean temperature is expected to respond to radiative forcing changes associated with increasing greenhouse gases and because it enhances the signal-to-noise ratio through averaging (for example, see Fig. 12.7 of Mitchell et al. 2001). Global-mean temperature is also a simple indicator used to compare internal climate variability from unforced climate model simulations with observations (for example, see Fig. 12.1 of Mitchell et al. 2001). Hence, global-mean temperature is commonly used as the simplest index of global climate variability and change.

K. Braganza · D.J. Karoly (✉)
School of Mathematical Sciences, Monash University,
PO Box 28M Clayton, VIC 3800 Australia
E-mail: david.karoly@sci.monash.edu.au

A.C. Hirst
CSIRO Atmospheric Research, Aspendale, VIC, Australia

M.E. Mann
Department of Environmental Sciences, University of Virginia,
Charlottesville, VA, USA

P. Stott · S.F.B. Tett
Hadley Centre for Climate Prediction and Research,
Meteorological Office, Bracknell, Berks., UK

R.J. Stouffer
Geophysical Fluid Dynamics Laboratory, Princeton, NJ, USA

There is additional information in the patterns of surface air temperature variations, apart from the global-mean. In this study, we use some other simple indices of surface temperature patterns, including the land–ocean temperature contrast, the meridional temperature gradient, the inter-hemispheric contrast, and the magnitude of the annual cycle, to describe global climate variability and change. These indices are associated with dynamical factors determining aspects of the large-scale atmospheric circulation. They are expected to contain information independent of the global-mean temperature for internal climate variations. The indices also represent the main features of the modelled surface temperature response to increasing greenhouse gases in the atmosphere. Hence, they should have a coherent response for greenhouse climate change.

Preliminary results from this study were presented by Karoly and Braganza (2001) but they are greatly extended here. We use global instrumental observations for 1880–1999, climate reconstructions from proxy data for 1700–1900, and simulations from five different coupled ocean–atmosphere climate models to investigate the variability and correlation structure of these indices on interannual and decadal time scales. The indices are used to evaluate the performance of control climate model simulations of internal climate variability. As the indices are expected to contain independent information for internal climate variations but show a coherent response to greenhouse forcing, the observed correlation structure of the indices is compared with forced and unforced model simulations.

The instrumental observational record is short (only about 120 years of useful information) and estimates of internal, natural climate variability may be affected by contamination of variability on all space and time scales by the response to anthropogenic forcing. Thus, we turn to two other data sources that give us complementary information about the variability of the indices, though each of these sources has its own limitations and uncertainties. Better statistics are available from the long model control simulations by taking multiple 120-year samples to provide an ensemble, and averaging the results from the ensemble to better estimate the statistics of interest and the uncertainty associated with using a single 120-year sample. Of course, this is only for the simulated climate and may not realistically represent the variability in the real climate. Longer and independent records of the indices from the real climate system are available from climate reconstructions from proxy data, which are used for the period 1700–1900. This provides a record that is almost twice the length of that from the instrumental data and is prior to the twentieth century, so it is much less likely to have been influenced by the climate response to anthropogenic forcing. Of course, the indices computed from the proxy data reconstructions have substantial uncertainties of their own, but these uncertainties are complementary to the uncertainties in the other two data sources. In particular, they avoid the potential contamination bias from the

response to anthropogenic forcing in using the instrumental data alone.

The observational and model data sets are described in the next section and the indices are defined in Sect. 3. The observed and modelled variability of the indices are compared in Sect. 4 and the correlation structure of the indices is examined in Sect. 5. Some conclusions on possible uses of these indices are presented in the final section.

This is the first part of a two-part study that seeks to examine the variations of the indices in observations over the last 120 years and in model simulations of unforced climate variability and the response to anthropogenic forcing. In the second part, we describe the observed trends in the indices and compare them with climate change simulations.

2 Datasets

2.1 Observations

2.1.1 Instrumental surface temperature

The observational data used here are a combined data set based on 5° resolution gridded surface air temperature anomalies over land (Jones 1994; Jones et al. 1999) and 5° gridded sea surface temperature anomalies (Parker et al. 1995). These data are obtained from quality controlled instrumental observations and have been used in a majority of recent studies in climate change, including the IPCC Second Assessment Report (SAR) (Nicholls et al. 1996) and IPCC TAR (Folland et al. 2001). These data are used for the period 1880–1999, with the period prior to 1880 excluded due to sparse coverage.

2.1.2 Paleo-climate reconstructions

In addition to the instrumental record described, the multi-proxy climate reconstructions of Mann et al. (2000a, b) have been used as a representation of surface temperature variations for the period 1700–1900. Previous studies have shown that these data can be useful in supplementing the more recent observed data and hence provide a longer context to recent observed climate variations (Bradley and Jones 1993; Mann et al. 1995, 1998; Jones et al. 1998; Folland et al. 2001).

Mann and colleagues used multi-proxy networks of high-resolution natural archives such as tree rings, ice cores, and corals, combined with long historical and instrumental records, to reconstruct climate patterns several centuries back in time. These include large-scale surface temperature patterns (Mann et al. 1999, 2000a, b), indices of the El Nino/Southern Oscillation ("ENSO") phenomenon (Mann et al. 2000a, b), the North Atlantic Oscillation (Cullen et al. 2001), and patterns of internal (Delworth and Mann 2000) and externally-forced (Waple et al. 2002) climate variability.

The Mann et al. approach to paleo-climate reconstruction has been discussed elsewhere in more detail (Mann et al. 1998, 1999, 2000a, b). The method involves a multivariate calibration of the leading eigenvectors of the twentieth century surface temperature record against a global network of diverse proxy indicators. This approach exploits the large-scale structure and complementary seasonal and climatic information in a diverse network of climate proxy indicators in reconstructing past global surface temperature patterns. Significant skill in these reconstructions has been indicated in independent cross-validation exercises (Mann et al. 1998, 1999, 2000a, b) and appropriate self-consistent uncertainties have been estimated back in time. The annual-mean reconstructions of

Mann et al. (1998) have recently been extended to include distinct warm and cold-season reconstructions (Mann et al. 2000b). From the reconstructed surface temperature patterns, global, hemispheric, or regional averages of interest are readily evaluated.

The methodology employed in these proxy-based climate reconstructions assumes that each proxy record exhibits a linear relationship with one or more of the principal components (PCs) of the instrumental surface temperature record. The methodology does not assume that the proxy record is itself necessarily an indicator of temperature. Only carefully screened records with annual resolution and dating were used. For the period after 1820, when all 112 records were available, it was possible to skillfully reconstruct 11 PCs, or temperature patterns, calibrating (and cross-validating) between 30–40% of the total instrumental surface temperature variance, and 70–80% of the instrumental variance in Northern Hemisphere (NH) mean temperature. For the period 1700–1900 over which the proxy based reconstructions are used in this study, they are approximately homogeneous in terms of the available proxy indicator network and resolved temperature variance at the largest scales (at least 60–70% of the NH mean temperature variance is resolved). The proxy reconstructions are used to estimate the same indices as the instrumental observations. The spatial details of the reconstructions are discussed elsewhere (Mann et al. 2000b; data available electronically through the NOAA Data Centre for Paleoclimatology).

2.2 Global climate models

Near-surface air temperature data from five coupled ocean–atmosphere climate models are included in this analysis. Each of the models was also used in the IPCC TAR (McAvaney et al. 2001). Very brief descriptions of the models are given.

2.2.1 The US Geophysical Fluid Dynamics Laboratory GCM (GFDL R30)

A spectral atmospheric model with rhomboidal truncation at wave number 30 equivalent to 3.75° longitude × 2.2° latitude (96 × 80) with 14 levels in the vertical. The atmospheric model is coupled to an 18 level gridpoint (192 × 80) ocean model where two ocean grid boxes under-lie each atmospheric grid box exactly. Both models are described by Delworth et al. (submitted 2001) and Delworth and Knutson (2000). The IPCC TAR nomenclature for this model is GFDL_R30_c.

2.2.2. The Australian CSIRO Mark 2 GCM (CSIRO Mk2)

An atmospheric R21 spectral model with an equivalent horizontal resolution 5.6° longitude × 3.2° latitude (64 × 56) and 9 levels in the vertical. This is coupled to a gridpoint ocean model of the same horizontal resolution with 21 vertical levels (Gordon and O'Farrell 1997; Hirst et al. 2000).

2.2.3. The UK Meteorological Office Hadley Centre GCMs (HadCM2 and HadCM3)

Both GCMs use the same atmospheric horizontal resolution, 3.75° × 2.5° (96 × 72) finite difference model (T42/R30 equivalent) with 19 levels in the atmosphere and 20 levels in the ocean (Johns 1996; Johns et al. 1997). For HadCM2, the ocean horizontal grid lies exactly under that of the atmospheric model. The resolution for the ocean component of HadCM3 has been greatly improved (1.25° × 1.25°) with six ocean grid boxes for every atmospheric grid box. In the context of results shown here, the main difference between the two models is that HadCM3 includes improved representations of physical processes in the atmosphere and the ocean (described by Gordon et al. 2000). For example, HadCM3 employs a radiation scheme that explicitly represents the radiative effects of minor greenhouse gases as well as CO_2, water vapour and ozone (Edwards and Slingo 1996), as well as a simple parametrization of background aerosol (Cusack et al. 1998).

2.2.4 The German Max-Planck-Institute fur Meteorologie GCM (ECHAM4/OPYC3)

An atmospheric T42 spectral model equivalent to 2.8° longitude × 2.8° latitude (128 × 64) with 19 vertical layers (Roeckner et al. 1996a). The ocean model OPYC3 uses isopycnals as the vertical coordinate system (Oberhuber 1993). As with HadCM3, ECHAM4 also explicitly represents the effects of a range of greenhouse gases and includes an explicit treatment for the radiative effects of aerosols. A full description of the coupled model can be found in Roeckner et al. (1996b).

All the GCMs include sea-ice models and representation of land-surface processes. CSIRO Mk2, GFDL R30 and HADCM2 all include seasonal adjustments of heat and fresh water fluxes at the surface to reduce climate drift in the coupled model simulations. ECHAM4 has annual mean flux adjustments only (heat and water) while HADCM3 has no flux adjustments and maintains a stable control climate simulation.

2.3 Model simulations

We use data from long control simulations with each of the models that have been performed without any change to the external forcing parameters. They therefore represent the intrinsic variability of the modelled coupled ocean–atmosphere system. The experiments from which we have data available are a 1000 year control simulation from CSIRO Mk2 (Hirst 1999; Hirst et al. 2000), 990 years of data from HadCM2 (Johns et al. 1997; Tett et al. 1997), 1830 years from HadCM3 (Collins et al. 2001; Johns et al. submitted 2002), 500 years from GFDL-R30 (Delworth et al. 2000) and 240 years from ECHAM4 (Roeckner et al. 1996).

We also make use of a series of simulations of the climate response to anthropogenic forcing. The radiative forcing experiments used here include anthropogenic changes in greenhouse gases and sulfate aerosols. For the CSIRO Mk2, GFDL and HadCM2 models, these changes are expressed as an increase in equivalent CO_2 according to IPCC scenario IS92a along with changes in anthropogenic sulfate aerosols represented through regional changes to surface albedo. For the HadCM3 and ECHAM4 models, increases in individual major anthropogenic greenhouse gases are included, together with explicit treatment of the direct radiative effect of sulfate aerosols. HadCM3 also includes a parameterization for indirect sulphate forcing effects via cloud albedo changes as well as a representation of anthropogenic changes to tropospheric and stratospheric ozone (Johns et al. 2002). From HadCM2 and HadCM3, we have four independent members of an ensemble of simulations with increasing greenhouse gases and sulfate aerosols (GS), three GS ensemble members from GFDL R30, two from ECHAM4 and one from CSIRO Mk2.

2.4 Data coverage

Observations over the past century are not uniform in their spatial coverage with large areas of missing data, particularly in the early part of the record. However the suitability of the observational data to estimate global climate variability has been reasonably established (Jones 1995; Parker et al. 1995). In order to overcome the differences in spatial coverage between the observations and models, a data mask was created to exclude regions where the observations were sparse or non-existent. This mask was applied to both observations and model data. Reasonable coverage in the observations was deemed to be areas that had at least 40 years of data since 1900. The year was defined as the four-season average from December to November, not the normal calendar year. A year was included for a grid box if at least two seasons had data present although, in practice, very

Fig. 1 Data mask used in the calculation of the indices from both observed and modelled data. *White areas* indicate regions included in the analysis. *Shaded areas* indicate regions of sparse coverage (less than 40 years of data since 1900) that were excluded from the analysis
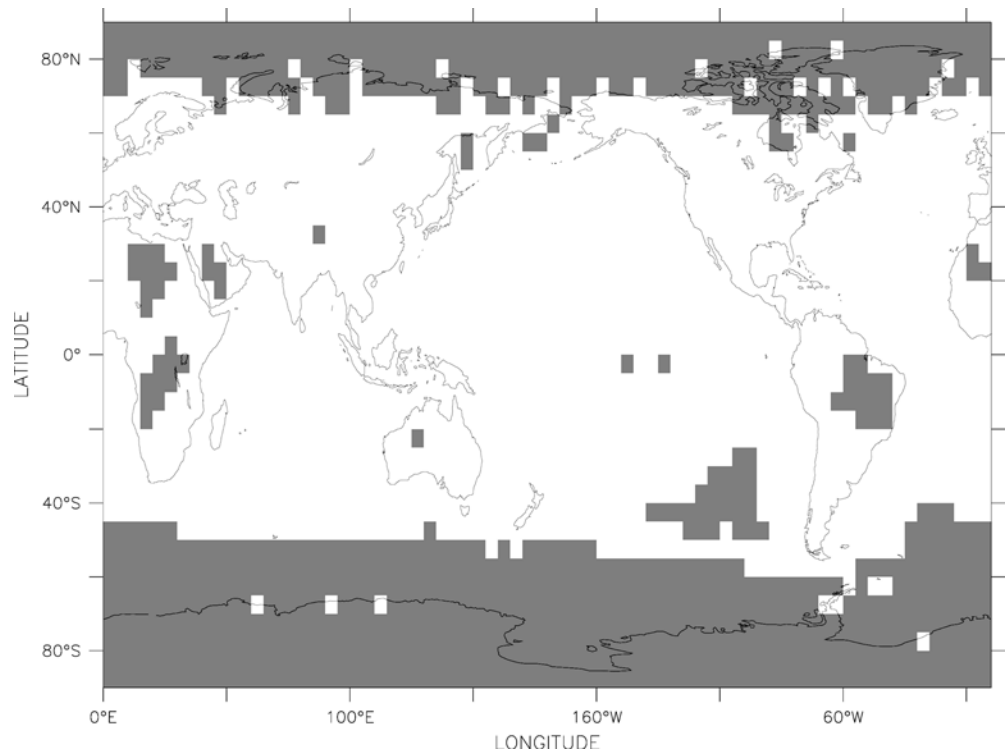
few of the grid boxes had less than three seasons with data in a single year. The variability of the December–November annual averages is almost identical to the variability of the calendar year annual means. The use of a fixed data mask over one that matched the temporal variation in data coverage was based on the fact that the sensitivity of the indices to variations in the mask was found to be small in both observations and control simulations. The data mask used in this study is shown in Fig. 1. As a result of applying the mask, large regions of the Southern Ocean and Antarctica, as well as smaller regions in the high northern latitudes and over the interior of the southern continents have been omitted from the analysis.

For the proxy based climate reconstructions, the indices are computed using the same data mask as the instrumental data but the effective resolution of the proxy data is much poorer. The resolved variance of the proxy reconstructions on smaller spatial scales is much less than at hemispheric scales in the Northern Hemisphere. The reliability of the proxy reconstructions is lower in the Southern Hemisphere and for seasonal variations, compared with annual mean variations. Hence, we would expect the indices from the proxy reconstructions to compare better with the instrumental observations for very large area-averages, such as for the global or hemispheric means, or for the land–ocean temperature contrast.

3 Defining the global indices

As outlined, we want to define simple global indices that capture the key features of the pattern of surface temperature change due to increasing greenhouse gases. In defining a number of indices, it is also important that each index be reasonably independent under internal, low frequency climate variability. In this manner, the indices can contribute additional information about the nature of the observed and modelled climate change and can also be considered together as a unique, collective signal. One of the main purposes here is to examine the

variability and correlation structure of the chosen indices in order to assess their suitability as independent indices of climate change.

Five simple indices based on surface temperature patterns are used. Apart from the global-mean temperature, all the other indices are based on differences of mean temperatures between different regions or times. Hence, by construction, variations of these indices are likely to not be strongly related to variations of global-mean temperature. All the indices have been identified previously in studies of climate variability and change, although they have not been considered together, except by Karoly and Braganza (2001). The surface temperature data are anomalies relative to a 30-year reference period from the control simulations for model data and relative to the period 1961–1990 in the observations (Jones 1994; Jones et al. 1999).

1. Global-mean surface temperature (GM): The area-weighted global average of surface temperature, which has been the parameter most commonly used in climate change studies.

2. The contrast between land and ocean surface temperature (LO): LO is defined as the difference between mean surface air temperature (SAT) over land and mean sea surface temperature (SST). This index has been chosen to capture the pattern of greater and more rapid warming over land than ocean (SAT – SST) that has been identified in previous studies (Jain et al. 1999; Meehl et al. 1993). LO is also a factor in large scale atmospheric circulation and has long been identified with the strength of the monsoons (Piexoto and Oort 1992).

3. The inter-hemispheric difference in surface temperature (NS): NS is defined as mean Northern Hemisphere (NH) temperature minus the mean Southern Hemisphere (SH) temperature. This index has been chosen to represent the influence of anthropogenic sulphate aerosols in the NH, which contribute to relative cooling in the NH (Kaufmann and Stern 1997; Meehl et al. 1993; Santer et al. 1996a; Wigley et al. 1998).

4. The mean magnitude of the annual cycle in temperature over land (AC): The magnitude of the annual cycle was calculated for each hemisphere by subtracting mean winter from mean summer surface temperature over land. These quantities were then area-weighted by the fraction of global land surface area in the respective hemisphere and combined into a single index.

$$AC = w_{NH}\langle JJA - DJF \rangle + w_{SH}\langle DJF - JJA \rangle$$

Note that AC is effectively the seasonal range between winter and summer temperatures and will be somewhat less than the magnitude of the annual cycle estimated by fitting a sinusoid to the monthly temperatures. The variations of AC computed here are highly correlated with those calculated from fitting a sinusoid to monthly data. For the proxy data, AC was estimated from the difference between warm season and cold season reconstructions, which will have slightly less variance than the summer minus winter seasonal differences.

AC has been chosen to represent the relative strength of seasonal warming in the observations which studies have suggested shows increased warming over land during winter (Thomson 1995; Mann and Park 1996).

5. The mean meridional temperature gradient in the NH mid-latitudes (MTG): MTG is defined as the difference of two zonal bands representing the NH mid to high latitudes (52.5°N–67.5°N) minus the NH sub-tropics (22.5°N–37.5°N). MTG has been chosen to represent the expected polar amplification of the warming due to increasing greenhouse gases (Manabe and Stouffer 1980; Wigley and Barnett 1990) and the recent observed pattern of greater warming in high latitudes compared to the tropics (Gitelman et al. 1997, 1999; Jain et al. 1999). It is also associated with the large-scale atmospheric circulation as a measure of baroclinicity and the strength of mid-latitude weather systems (Piexoto and Oort 1992). A positive trend in MTG corresponds with a decrease in the magnitude of the normal temperature decrease with latitude in the NH.

4 Climate variability

In this section, the observed variability of the indices on interannual and decadal time scales is compared with the variability in the control and forced climate model simulations. In this manner, we evaluate the quality of the coupled model simulations of internal climate variability. This variability is estimated using the standard deviation of the indices. To estimate the variability on decadal time scales, the time series of the annual values of the indices are filtered with a low pass, 21 point binomial filter (half power at periods of 10 years) as used in IPCC TAR (Folland et al. 2001).

As there are significant observed trends in the indices over the twentieth century (Karoly and Braganza 2001), these trends must be removed to obtain an estimate of the unforced climate variability from the observational data. A polynomial (4th order) trend was fitted to the 120-year (1880–1999) time series of each of the observed indices. The residuals, after removing this trend, are taken as the detrended observations and used to estimate the internal or unforced variability of the observed climate. The variability of the detrended indices for this 120-year period is compared with 120-year samples from the long control climate integrations and with the variability estimated from the proxy data reconstructions. These are in turn compared with the variability of recent observed climate (with the trends included) and with those of the forced model experiments. The results for the detrended observations prove to be relatively insensitive to the order of the polynomial used to represent the century-scale trend. However, as higher-order polynomials are used to represent the trend, more of the low-frequency (decadal) variability is assigned to the century scale trend and less is included in the residuals.

A comparison of the recent observations with estimates of past climate variability is illustrated in Fig. 2, which shows low-frequency variations in each of the indices from proxy data, recent instrumental observations and the detrended observations. The significant trends in the indices during the last 50 to 100 years are reconstructed with good accuracy by the proxy data for four of the five indices, GM, LO, MTG and NS. While no significant trends exist in the paleo-climate reconstructions prior to the twentieth century, the decadal variability of the proxy data for the period 1700–1900 compares well with that of the recent detrended observations. For the annual cycle index, the proxy data underestimates the decadal variability and shows no recent trend, unlike that observed. This result reflects the inability of the paleo-climate reconstructions to accurately resolve seasonal scale temperature variability.

While Fig. 2 may indicate that the detrending method applied here is reasonable, a more quantitative assessment is necessary if we are to use such estimates to evaluate the simulated unforced variability of the climate models. Since the influence of external forcing may affect variability at all temporal and spatial scales (Hu et al. 2001; Meehl et al. 2000), removal of the non-linear trend does not guarantee that the residuals accurately represent internal climate variability. In order to test the effectiveness of the detrending method, time series of the indices from the GS-forced simulations with the CSIRO Mk2 and HadCM2 models were detrended and compared with intrinsic variability estimates from control climate simulations, paleo-climate reconstructions and the recent detrended observations. In all of the climate models used
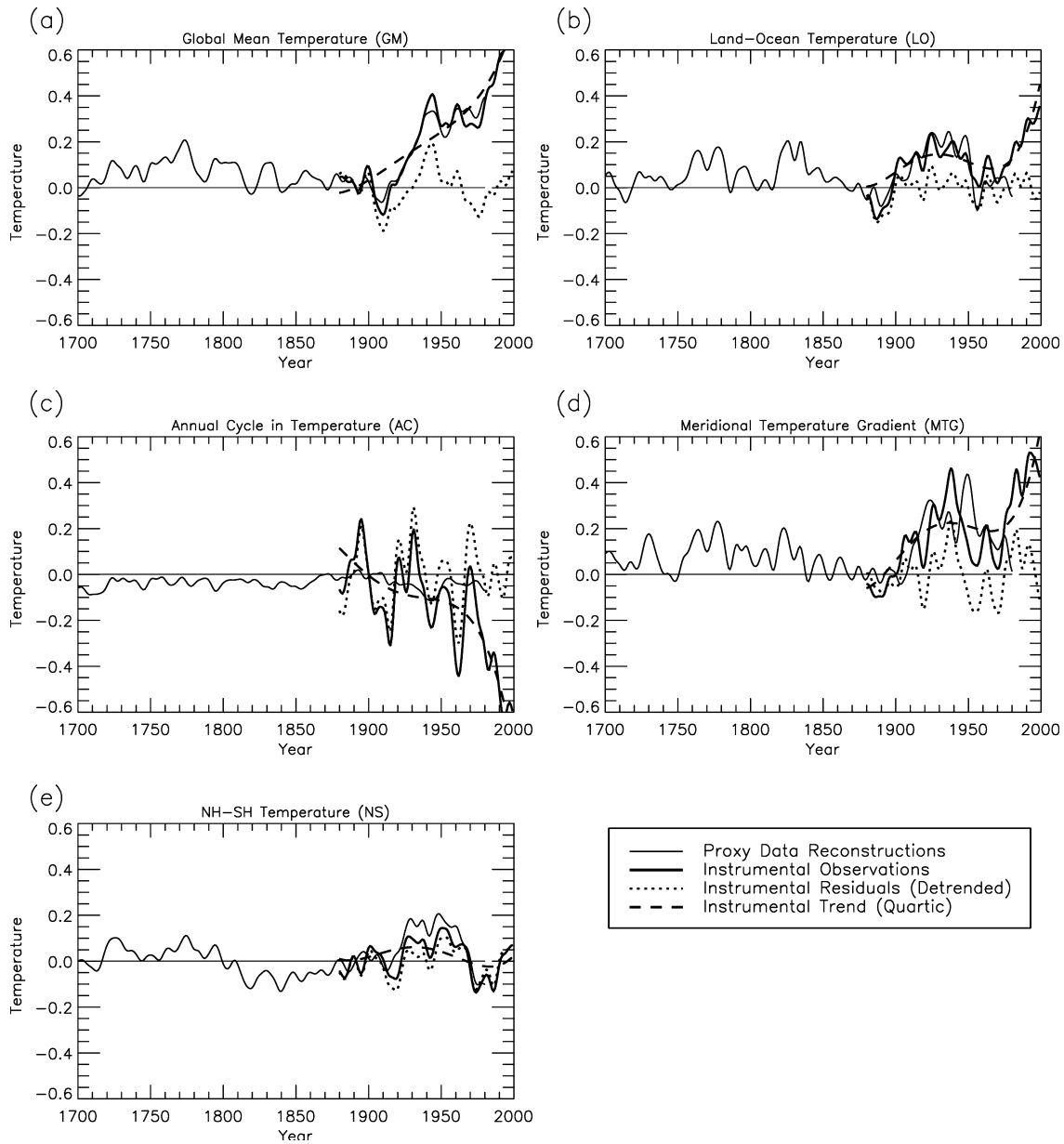
Fig. 2a–e Low-pass filtered (decadal) time series of each of the indices from proxy data reconstructions (1700–1980) and instrumental observations (1880–1999). Also shown are the 4th order polynomial trend fitted to the instrumental observations and the low-pass filtered residual from this trend, which represent the decadal, detrended observed time series

here, no significant trends exist in any of the indices of the long control integrations and hence, no detrending has been applied to the timeseries of these indices. Similarly, as shown above and in Fig. 2, the paleo-climate indices for the period 1700–1900 also show no significant trends and are therefore not detrended. The absence of large linear trends in global temperature during this period is common to several different paleoreconstructions (for example, see Briffa et al. 2001) and is most likely related to a lack of significant trends in radiative forcing (Crowley 2000). Proxy data reconstructions for the period after 1900 are not included in the analysis. Table 1 and Fig. 3a show the interannual and decadal standard deviations, respectively, of the indices for the detrended forced model simula-

tions for the period 1880–1999 and for the different estimates of internal climate variability. Standard deviations of the control model runs are estimated using the mean standard deviation of overlapping 120-year samples taken at 50-year intervals. Also shown are the estimated 90% confidence intervals, based on the student t distribution, for the standard deviation. These uncertainty estimates are derived from the multiple 120-year samples from the long control simulations, excluding ECHAM4 for which we have only 240 years of data.

The standard deviations of the detrended GS residuals are compared with those from the control simulations in Table 1. For both models and for all the indices and their components, the variability of the detrended

Table 1a Standard deviations of decadal variations (in °C) in each of the indices and their components from observations, detrended observations, proxy climate reconstructions, and control (CL) and GS-forced model simulations. The indices are the global mean temperature (GM), land–ocean temperature contrast (LO), interhemispheric temperature contrast (NS), magnitude of the annual cycle over land (AC), and meridional temperature gradient in the NH (MTG). Error estimates represent uncertainty at the 90% confidence interval based on resampling from the long control simulations

	Observations	Observations (det)	Proxy	CSIRO Mk2 CL	CSIRO Mk2 GS (det)	HadCM2 CL	HadCM2 GS (det)	HadCM3 CL	GFDLR30 CL	ECHAM4 CL
GM	0.20	0.08	0.05	0.05 ± 0.01	0.04	0.07 ± 0.02	0.07	0.06 ± 0.01	0.07 ± 0.02	0.06
Land	0.26	0.09	0.09	0.07 ± 0.02	0.06	0.10 ± 0.04	0.11	0.09 ± 0.02	0.10 ± 0.03	0.09
Ocean	0.19	0.08	0.07	0.04 ± 0.01	0.04	0.06 ± 0.02	0.06	0.05 ± 0.01	0.07 ± 0.01	0.05
LO	0.11	0.06	0.06	0.06 ± 0.01	0.05	0.06 ± 0.02	0.07	0.06 ± 0.02	0.06 ± 0.02	0.07
NH	0.21	0.09	0.07	0.07 ± 0.02	0.06	0.08 ± 0.03	0.08	0.08 ± 0.03	0.09 ± 0.02	0.07
SH	0.20	0.07	0.04	0.04 ± 0.01	0.03	0.07 ± 0.02	0.07	0.06 ± 0.03	0.07 ± 0.02	0.08
NS	0.07	0.06	0.06	0.06 ± 0.02	0.05	0.07 ± 0.03	0.07	0.09 ± 0.06	0.07 ± 0.02	0.09
NH jja	0.21	0.11	0.04	0.09 ± 0.03	0.08	0.11 ± 0.04	0.11	0.08 ± 0.01	0.11 ± 0.02	0.08
NH djf	0.41	0.16	0.04	0.12 ± 0.03	0.12	0.16 ± 0.06	0.15	0.16 ± 0.05	0.16 ± 0.02	0.19
AC	0.21	0.13	0.02	0.09 ± 0.02	0.08	0.12 ± 0.04	0.10	0.12 ± 0.04	0.12 ± 0.03	0.12
MTG	0.17	0.10	0.06	0.16 ± 0.04	0.13	0.14 ± 0.04	0.15	0.15 ± 0.03	0.14 ± 0.02	0.16

Table 1b Standard deviations of interannual variations (in °C) in each of the indices and their components, as in a

	Observations	Observations (det)	Proxy	CSIRO Mk2 CL	CSIRO Mk2 GS (det)	HadCM2 CL	HadCM2 GS (det)	HadCM3 CL	GFDLR30 CL	ECHAM4 CL
GM	0.23	0.13	0.08	0.07 ± 0.01	0.07	0.13 ± 0.02	0.13	0.12 ± 0.01	0.14 ± 0.02	0.09
Land	0.33	0.20	0.15	0.14 ± 0.02	0.14	0.19 ± 0.03	0.20	0.19 ± 0.02	0.21 ± 0.02	0.18
Ocean	0.21	0.12	0.10	0.06 ± 0.01	0.06	0.12 ± 0.02	0.12	0.10 ± 0.01	0.13 ± 0.03	0.07
LO	0.19	0.17	0.12	0.12 ± 0.01	0.14	0.14 ± 0.02	0.15	0.14 ± 0.01	0.14 ± 0.01	0.16
NH	0.24	0.15	0.10	0.10 ± 0.02	0.10	0.13 ± 0.02	0.14	0.13 ± 0.02	0.17 ± 0.02	0.11
SH	0.23	0.12	0.07	0.06 ± 0.01	0.06	0.16 ± 0.02	0.16	0.13 ± 0.02	0.15 ± 0.03	0.10
NS	0.12	0.11	0.08	0.09 ± 0.01	0.09	0.14 ± 0.02	0.15	0.13 ± 0.05	0.14 ± 0.02	0.12
NH jja	0.28	0.20	0.06	0.18 ± 0.02	0.17	0.26 ± 0.02	0.29	0.21 ± 0.02	0.26 ± 0.01	0.18
NH djf	0.65	0.52	0.06	0.31 ± 0.04	0.31	0.37 ± 0.04	0.38	0.39 ± 0.04	0.39 ± 0.03	0.49
AC	0.43	0.30	0.04	0.26 ± 0.03	0.24	0.33 ± 0.03	0.35	0.31 ± 0.02	0.34 ± 0.02	0.35
MTG	0.34	0.31	0.14	0.34 ± 0.04	0.33	0.32 ± 0.04	0.31	0.30 ± 0.03	0.35 ± 0.04	0.35

indices from the GS-forced simulations is not significantly different from the control simulations. This suggests that the long-term signal of GS forcing can be removed by the polynomial detrending. The variability of the detrended observations compares very well with the control climate simulations and proxy climate data for each of the indices and their components. In general, the standard deviation of the detrended observations is within the 90% confidence interval of the control run standard deviation for all the models at both interannual and decadal time scales. There are a small number of exceptions, such as the models generally underestimating the interannual variability of NH land temperature in winter and the interannual variability of the land–ocean temperature contrast. The decadal variability of MTG is found to be significantly larger in all the model simulations in comparison with observations. The reasons for this are unclear, as the interannual variability of MTG in the models is not significantly larger than observed. In terms of model comparison, CSIRO Mk2 has slightly less variability than the other models, perhaps because of its lower resolution. There do not appear to be consistent differences between the variability simulated by HadCM3, with no flux adjustment, and that simulated by the GFDL, HadCM2 and ECHAM models, which include flux adjustment.

Even though one may expect climate models to reasonably simulate the variability of global-scale parameters, it is a significant validation that these quite different models should so accurately simulate the variability of all the indices and their components. For some of the indices, the standard deviation from the proxy data underestimates the variability in the detrended observations and the control model simulations. This occurs for the variability of the seasonal temperatures over land, the magnitude of the annual cycle (AC), and the meridional temperature gradient (MTG). As noted by Mann et al. (2002b), the seasonal proxy reconstructions seriously underestimate the temperature variance, even on the largest scales.

Figure 3b shows the decadal standard deviations of the observed indices (trend included) from 1881–1999 compared with the ensemble-average standard deviation of forced GS runs over the same simulated period. Error estimates are based on the maximum range of values from different ensemble members for HadCM2, Had-CM3 and GFDL R30. For CSIRO Mk2 (single GS run) and ECHAM4 (2 ensemble members), no error estimates were calculated due to the small number of ensemble members. As expected, the indices show increased decadal standard deviations under anthropogenic forcing compared to the control simulations. This increase is largely due to the inclusion of century scale trends in all of the indices in both observations and GS simulations (Karoly and Braganza 2001). The magnitude of decadal variability is also similar for observations and models. For the annual cycle, the observed standard deviation is greater than that for GS forcing and is associated with an observed trend in AC that is
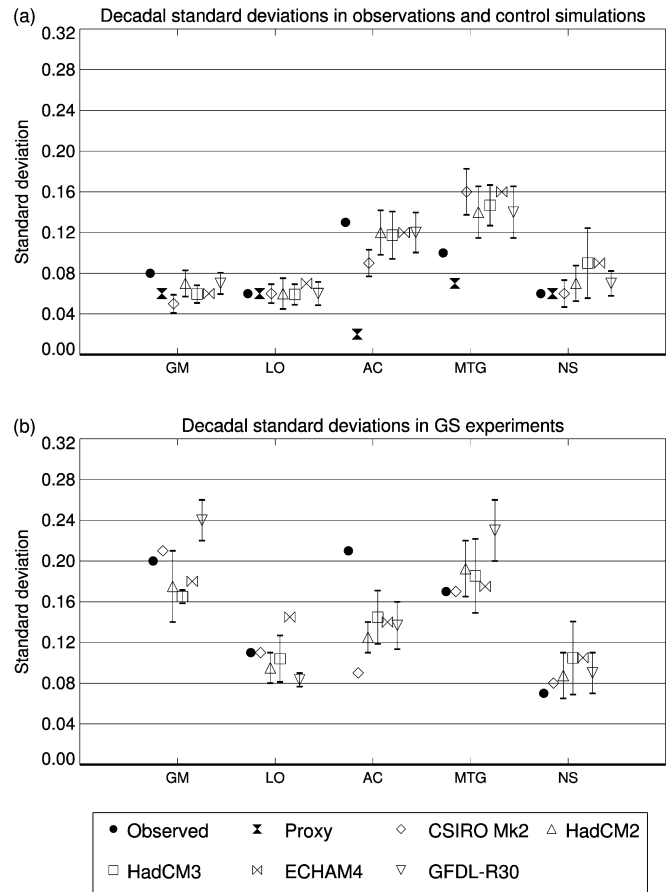

Fig. 3 Standard deviations (in °C) of decadal variations of the indices from: **a** detrended observations and control model simulations. Error bars represent uncertainty at the 90% confidence interval estimated by resampling the long control simulations. **b** Observations and GS-forced model simulations. Error bars represent uncertainty associated with the range of values from individual ensemble members. The indices are the global mean temperature (GM), land–ocean temperature contrast (LO), inter-hemispheric temperature contrast (NS), magnitude of the annual cycle over land (AC), and the meridional temperature gradient in the NH (MTG)

larger than the model simulations for the same period (Karoly and Braganza 2001). Investigating the signal of climate change on decadal to century time scales is likely to be better served through the comparison of the magnitude and time evolution of any trends in the indices. As outlined earlier, this will be the subject of a subsequent paper.

5 Relative correlations of the indices

Next, we consider the correlations between the indices associated with decadal and interannual variations. As mentioned earlier, in order to have an appropriate set of climate change indices, each must be reasonably independent for internal climate variability. Table 2 and Fig. 4a show the interannual and decadal timescale correlations, respectively, of the indices and their com-

Table 2 Correlations of interannual variations in the indices with global mean temperature (GM) from observations, detrended observations, paleo-climate (proxy) reconstructions and control model simulations. Error estimates represent uncertainty at the 90% confidence interval

	Observations	Observations (det)	Proxy	CSIRO Mk2 CL	HadCM2 CL	HadCM3 CL	GFDLR30 CL	ECHAM4 CL
Land	0.92	0.81	0.87	0.86 ± 0.03	0.87 ± 0.03	0.87 ± 0.03	0.91 ± 0.02	0.86
Ocean	0.98	0.94	0.84	0.85 ± 0.03	0.95 ± 0.01	0.94 ± 0.02	0.96 ± 0.01	0.87
LO	0.48	0.29	0.39	0.56 ± 0.08	0.38 ± 0.14	0.45 ± 0.10	0.48 ± 0.10	0.59
NH	0.98	0.95	0.97	0.94 ± 0.02	0.89 ± 0.02	0.88 ± 0.06	0.93 ± 0.02	0.88
SH	0.95	0.87	0.81	0.73 ± 0.10	0.88 ± 0.04	0.83 ± 0.11	0.84 ± 0.06	0.74
NS	0.16	0.32	0.54	0.52 ± 0.09	−0.17 ± 0.20	0.06 ± 0.19	0.24 ± 0.18	0.21
NH jja	0.82	0.66	0.62	0.60 ± 0.10	0.47 ± 0.14	0.44 ± 0.26	0.63 ± 0.07	0.64
NH djf	0.70	0.47	0.76	0.46 ± 0.12	0.30 ± 0.16	0.27 ± 0.14	0.41 ± 0.08	0.56
AC	−0.42	−0.19	−0.26	−0.11 ± 0.14	0.04 ± 0.17	0.01 ± 0.13	0.02 ± 0.07	−0.35
MTG	0.44	0.26	0.17	0.29 ± 0.15	0.26 ± 0.13	0.35 ± 0.14	0.29 ± 0.20	0.45

ponents with the global-mean temperature (GM) in the detrended observations, proxy data, and control climate model simulations. Once again, it is notable how well the models simulate the magnitude or at least *relative* strengths of the correlations with GM. Since the global-mean temperature is the area-weighted sum of the land and ocean temperatures, it is not surprising that both land and ocean temperature variations are closely related to variations of GM. However, the land–ocean contrast (LO) is not closely related to GM because, by construction, it is the difference between the land and ocean temperatures. Similarly for NS, AC and their respective components. Under GS forcing (Fig. 4b), the correlations of the LO, AC and MTG indices with GM are much greater than under internal variability in the model experiments and in the recent observations. This increase in correlation is associated with the common response of the indices to GS forcing in the model simulations, leading to trends in all these indices. The exception here is the annual cycle of CSIRO Mk2 which shows no clear signal under GS forcing, and of ECHAM4, which shows too much association with GM under internal variability. HadCM2 is perhaps the best performing model across all of the indices and their components.

In the case of the interhemispheric temperature contrast (NS), the correlation of the index with GM is highly variable between the different models for both the forced and unforced cases. For HadCM2 and HadCM3, NS also shows large variability between individual ensemble members in the GS simulations. The variability of NS may be associated with sensitivity to the temporal changes in the relative strengths of greenhouse gas and sulfate aerosol forcing (Santer et al. 1996b), as well as sensitivity to the simulated ocean heat uptake in the Southern Hemisphere (Karoly and Braganza 2001). Here, NS was also found to be highly correlated with LO in simulations of internal variability, particularly on decadal time scales (Table 3), although this structure is not seen in the observations or proxy data. The correlation in the models is likely due to the larger land fraction in the NH, particularly for the masked region that we are considering. As we are trying to identify indices that are independent of each other for natural climate variations and have a clear signal of anthropogenic climate change, the NS index does not satisfy these criteria and is not considered further here.

As a further test of the correlation structure of the indices, the inter-dependence of the indices is also investigated. This has been done by calculating the determinant of the correlation matrix of the indices GM, LO, AC and MTG on decadal time scales. The value of the determinant gives an estimate of the relative strength of the association between the indices. By definition, if all the indices are totally independent, the determinant equals unity while if any one of the indices is linearly dependent (highly correlated) with any other, the determinant falls to zero. Figure 5 shows the determinant
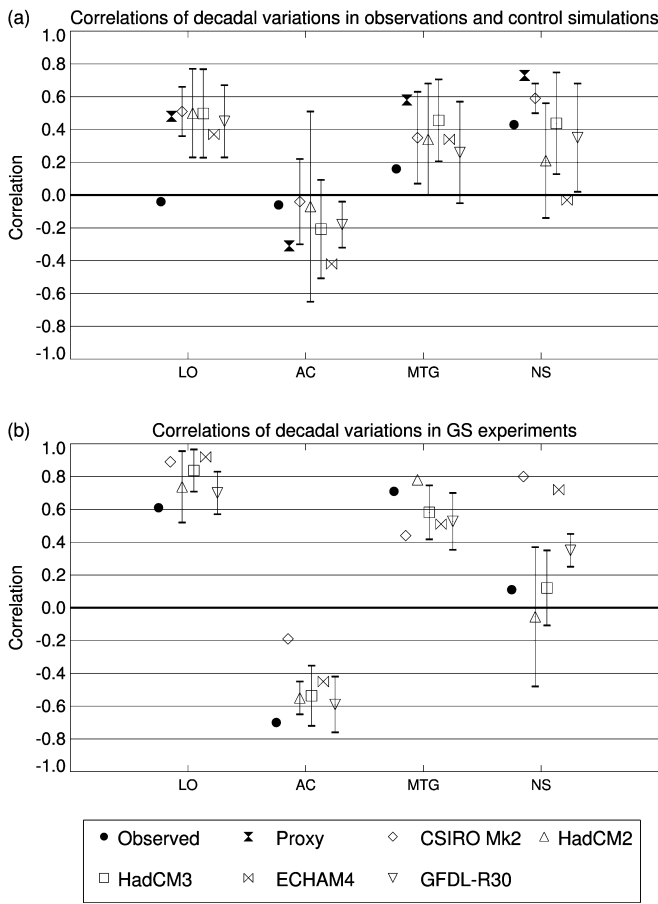
Fig. 4 Correlations of decadal variations of the indices with global-mean temperature (GM) from: **a** detrended observations and control model simulations. Error bars represent uncertainty at the 90% confidence interval. **b** Observations and GS-forced model simulations. Error bars represent uncertainty associated with the range of values from individual ensemble members

Fig. 5 Determinants of the correlation matrices for decadal variations of GM, LO, AC, and MTG from observations, control model simulations and GS-forced model simulations. *Error bars* in the *left hand group* represent 90% confidence intervals from resampling the long control runs while *those* in the *right hand group* represent the ranges of values between individual members of GS ensembles

Table 3 Correlations of interannual and decadal variations in interhemispheric temperature contrast (NS) with land–ocean temperature contrast (LO) from observations and control simulations

Data	Interannual	Decadal
Observations	0.48	–0.07
Observations (detrend)	0.51	0.06
Proxy	0.31	0.17
CSIRO Mk2	0.72 ± 0.08	0.68 ± 0.16
HadCM2	0.61 ± 0.12	0.65 ± 0.21
HadCM3	0.50 ± 0.13	0.73 ± 0.10
GFDL-R30	0.65 ± 0.06	0.75 ± 0.18
ECHAM4	0.63	0.73

of the correlation matrix on decadal time scales under internal variability (control integrations, proxy data 1700–1900 and detrended observations) and for GS forcing over the last 120 years (1880–1999). For almost all the control model cases and the detrended observations, it can be seen that, while there is by no means total independence between the indices, the determinant is
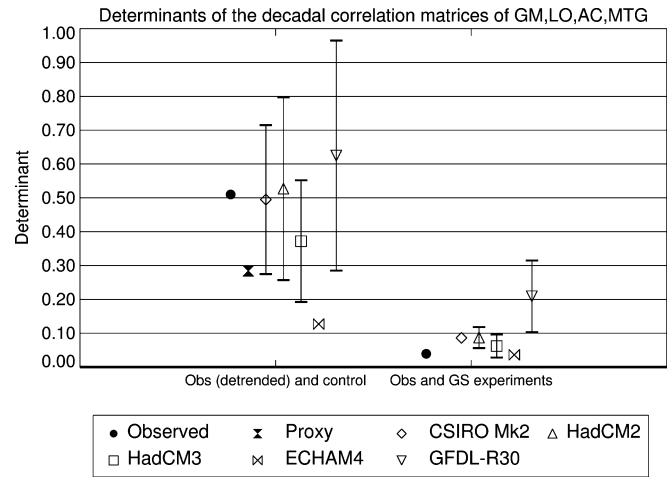
significantly higher than zero for internal climate variations. The only exception to this is the much shorter time series of ECHAM4. More importantly, there is a significant reduction in the magnitude of the determinant and hence much stronger coherence between the indices in the observations and GS runs over the twentieth century. This coherence between the indices is due to the common response of the indices to GS forcing in the models, leading to the trends in all these indices during the twentieth century. As the signal of climate change increases into the twentyfirst century, the determinant falls to zero in all model cases.

6 Discussion

We have defined a set of simple indices of surface air temperature patterns to describe global climate variability in observational data and climate model simulations. These are the global-mean temperature (GM), the land–ocean contrast (LO), the meridional gradient (MTG), the interhemispheric contrast (NS), and the magnitude of the annual cycle (AC). Since enhancement of the signal-to-noise ratio is improved by considering large spatial scales (Wigley and Barnett 1990; Stott and Tett 1998), defining indices based on large area averages increases the probability of climate change detection. The indices are also associated with dynamical factors that influence the large-scale circulation of the atmosphere. On interannual and decadal time scales, these indices contain information independent of the variations of the global-mean temperature for unforced climate variability. The five GCMs perform surprisingly well in simulating the magnitude of the variability and correlation structure of the indices for internal climate

variations, in comparison with detrended observations and proxy climate reconstructions. Hence, the indices provide a simple but effective way to evaluate global-scale climate variability in control climate model simulations.

Four of the five indices discussed here; GM, LO, AC and MTG, prove to be useful indicators of anthropogenic climate change. In the same manner as spatial fingerprints, such a set of global climate indices provides a coherent signal of anthropogenic climate change. This signal is apparent not only in the variability and trends of the indices but also in the apparent associations or covariability.

As expected, there is a significant increase in standard deviation on decadal and longer time scales in the recent observations when compared with detrended observations, simulated unforced climate variability, and variability in the proxy record between 1700 and 1900. This increase is well captured by GS experiments in the range of different models we have shown here and is associated with the trends in the observations and the GS-forced simulations. Of the four indices, the magnitude of change in AC is perhaps the least well simulated by the models.

In terms of correlation structure, the indices do not have a strong association with global mean temperature or each other under internal variability. This is not the case during the last 120 years of observations, where the long-term trends in the indices are highly correlated. As with the variability, this relationship is simulated by the GS experiments in all of the models. This change in the correlation structure is due to the coherent response of the indices to anthropogenic forcing in the model simulations, with trends in all the indices during the twentieth century.

In an attribution context, the change in the relationship between the indices may be a useful tool in distinguishing between different climate forcing mechanisms. This is true from a physical as well as statistical viewpoint as the indices themselves represent important physical processes. It remains for further study to investigate the time evolution of changes in the indices under unforced and anthropogenic climate variability and to include different radiative forcing experiments such as changes to the solar cycle and natural changes in stratospheric aerosols. This will be considered further in Part II of this study.

There are other simple indices of climate variability and change that may have similar properties to those used here. These include the temperature contrast between the troposphere and lower stratosphere (Karoly 1989; Karoly et al. 1994; Santer et al. 1996a) and the diurnal temperature range (Folland et al. 2001; Risbey et al. 2000). They have not been used in this study because quite different datasets are needed for those indices.

References

Bradley RS, Jones PD (1993) "Little Ice Age" summer temperature variations: their nature and relevance to recent global warming trends. The Holocene 3: 367–376

Briffa KR, Osborne TJ, Schweingruber FH, Harris IC, Jones PD (2001) Low-frequency temperature variations from a northern tree ring density network. J Geophys Res 106: 2929–2941

Collins M, Tett SFB, Cooper C (2001) The internal climate variability of HadCM3, a version of the Hadley Centre coupled model without flux adjustments. Clim Dyn 17: 61–81

Crowley TJ (2000) Causes of climate change over the past 1000 years. Science 289: 270–277

Cullen H, D'Arrigo R, Cook E, Mann ME (2001) Multiproxy-based reconstructions of the North Atlantic Oscillation over the past three centuries. Paleoceanography 15: 27–39

Cusack S, Slingo A, Edwards JM, Wild M (1998) The radiative impact of a simple aerosol climatology on the Hadley Centre GCM. QJR Meteorol Soc 124: 2517–2526

Delworth TL, Knutson TR (2000) Simulation of early 20th century global warming. Science 287: 2246–2250

Delworth TD, Mann ME (2000) Observed and simulated multidecadal variability in the North Atlantic. Clim Dyn 16: 661–676

Delworth TL, Stouffer RJ, Dixon KW, Spelman MJ, Knutson TR, Broccoli AJ, Kushner PJ, Wetherald RT (2002) Review of simulations of climate variability and change with the GFDL R30 coupled model. Clim Dyn 19: 555–574

Edwards JM, Slingo A (1996) Studies with a flexible new radiation code. I: choosing a configuration for a large scale model. QJR Meteorol Soc 122: 689–719

Folland CK, Karl TR, Christy JR, Clarke RA, Gruza GV, Jouzel J, Mann ME, Oerlemans J, Salinger MJ, Wang S-W (2001) Observed Climate Variability and Change. In: Houghton, JT, Ding Y, Griggs DJ, Noguer M, van der Linden PJ, Dai X, Maskell K, Johnson CA (eds) Climate change 2001: the scientific basis, Contribution of Working Group 1 to the Third Assessment Report of the Intergovernmental Panel on Climate Change. Cambridge University Press, Cambridge, UK, pp 99–182

Gitelman AI, Risbey JR, Kass RE, Rosen RD (1997) Trends in the surface meridional temperature gradient. Geophys Res Lett 24: 1243–1246

Gitelman AI, Risbey JR, Kass RE, Rosen RD (1999) Sensitivity of a meridional temperature gradient index to latitudinal domain. J Geophys Res 104: 16,709–16,717

Gordon C, Cooper C, Senior CA, Banks HT, Gregory JM, Johns TC, Mitchell JFB, Wood RA (2000) The simulation of SST, sea ice extents and ocean heat transports in a version of the Hadley Centre coupled model without flux adjustments. Clim Dyn 16: 147–168

Gordon HB, O'Farrell SP (1997) Transient climate change in the CSIRO coupled model with dynamic sea-ice. Mon Weather Rev 125: 875–907

Hirst AC (1999) The Southern Ocean response to global warming in the CSIRO coupled ocean–atmosphere model. Environ. Model Software: Spec Iss on Modelling Global Climatic Change. 14: 227–242

Hirst AC, O'Farrell SP, Gordon HB (2000) Comparison of a coupled ocean–atmosphere model with and without oceanic eddy-induced advection. 1. Ocean spin-up and control integrations. J Clim 13: 139–163

Houghton JT, Ding Y, Griggs DJ, Noguer M, van der Linden PJ, Dai X, Maskell K, Johnson CA (eds) Climate Change 2001: the scientific basis, Contribution of Working Group 1 to the Third Assessment Report of the Intergovernmental Panel on Climate Change. Cambridge University Press, Cambridge, United Kingdom, pp 881

Hu Z-Z, Bengtsson L, Roeckner E, Christoph M, Bacher A, Oberhuber JM (2001) Impact of global warming on the inter-annual and interdecadal climate modes in a coupled GCM. Clim Dyn 17: 361–374

Jain S, Lall U, Mann ME (1999) Seasonality and interannual variations of Northern Hemisphere temperature: Equator to pole temperature gradient and land–ocean contrast. J Clim 12: 1086–1100

Johns TC, Carnell RE, Crossley JF, Gregory JM, Mitchell JFB, Senior CA, Tett SFB, Wood RA (1997) The second Hadley Centre coupled ocean–atmosphere GCM: model description, spin-up and validation. Clim Dyn 13: 103–134

Johns TC (1996) A description of the Second Hadley Centre Coupled Model (HadCM2). Climate Research Technical Note 71, Hadley Centre, United Kingdom Meteorological Office, Bracknell Berkshire RG12 2SY, UK, pp 19

Jones PD (1994) Hemispheric surface air temperature variations: a reanalysis and update to 1993. J Clim 7: 1794–1802

Jones PD (1995) Land surface temperatures – Is the network good enough? Clim Change 31: 545–558

Jones PD, Briffa KR, Barnett TP, Tett SFB (1998) High-resolution paleoclimate records for the last millennium: interpretation, integration and comparison with General Circulation Model control-run temperatures. The Holocene 8: 455–471

Jones PD, New M, Parker DE, Martin S, Rigor IG (1999) Surface air temperature and its changes over the past 150 years. Rev Geophys 37: 173–199

Karoly DJ (1989) Northern Hemisphere temperature trends: a possible greenhouse gas effect? Geophys Res Lett 16: 465–468

Karoly DJ, Braganza K (2001) Identifying global climate change using simple indices. Geophys Res Lett 28: 2205–2208

Karoly DJ, Cohen JA, Meehl GA, Mitchell JFB, Oort AH, Stouffer, RJ, Wetherald RT (1994) An example of fingerprint detection of greenhouse climate change. Clim Dyn 10: 97–105

Kaufmann RK, Stern DI (1997) Evidence for human influence on climate from hemispheric temperature relations. Nature 388: 39–44

Manabe S, Stouffer RJ (1980) Sensitivity of a global climate model to an increase in the CO_2 concentration in the atmosphere. J Geophys Res 85: 5529–5554

Mann ME, Park J (1996) Greenhouse warming and changes in the seasonal cycle of temperature: Model versus observations. Geophys Res Lett 23: 1111–1114

Mann ME, Park J, Bradley RS (1995) Global interdecadal and century-scale climate oscillations during the past five centuries. Nature 378: 266–270

Mann ME, Bradley RS, Hughes MK (1998) Global-scale temperature patterns and climate forcing over the past six centuries. Nature 392: 779–787

Mann ME, Bradley RS, Hughes MK (1999) Northern Hemisphere temperatures during the past millennium: inferences, uncertainties, and limitations. Geophys Res Lett 26: 759–762

Mann ME, Bradley RS, Hughes MK (2000a) Long-term variability in the El Nino Southern Oscillation and associated teleconnections. In: Diaz HF, Markgraf V (eds) El Nino and the Southern Oscillation: multiscale variability and its impacts on natural ecosystems and society. Cambridge University Press, Cambridge, UK, pp 357–412

Mann ME et al (2000b) Annual temperature patterns in past centuries: an interactive presentation. Earth Interactions 4-4: 1–29

McAvaney BJ, Covey C, Joussaume S, Kattsov V, Kitoh A, Ogana W, Pitman AJ, Weaver AJ, Wood RA, Zhao Z-C (2001) Model

Evaluation. In: Houghton JT, Ding Y, Griggs DJ, Noguer M, van der Linden PJ, Dai X, Maskell K, Johnson CA (eds) Climate change 2001: the scientific basis. Contribution of Working Group 1 to the Third Assessment Report of the Intergovernmental Panel on Climate Change. Cambridge University Press, Cambridge, UK, pp 471–524

Meehl GA, Washington WM, Karl TM (1993) Low-frequency variability and CO_2 transient climate change: Part 1. Time-averaged differences. Clim Dyn 8: 117–133

Meehl GA, Washington WM, Arblaster JM, Bettge TW, Strand WG (2000) Anthropogenic forcing and decadal climate variability in sensitivity experiments of 20th and 21st century climate. J Clim 13: 3728–3744

Mitchell JFB, Karoly DJ, Allen MR, Hegerl G, Zwiers F, Marengo J (2001) Detection of climate change and attribution of causes. In: Houghton JT et al (eds) Climate change 2001: the scientific basis. Contribution of Working Group I to the Third Assessment Report of the Intergovernmental Panel on Climate Change. Cambridge University Press, Cambridge, UK, pp 695–738

Nicholls N, Gruza GV, Jouzel J, Karl TR, Ogallo LA, Parker DE (1996) Observed climate variability and change. In: Houghton JT et al (eds) Climate change 1995: the science of climate change. Cambridge University Press, Cambridge, UK, pp 133–192

Oberhuber JM (1993) The OPYC ocean general circulation model. Techn Rep 7, Deutsches Klimarechenzentrum, Hamburg, Germany

Parker DE, Folland CK, Jackson M (1995) Marine surface temperature: observed variations and data requirements. Clim Change 31: 559–600

Piexoto JP, Oort AH (1992) Physics of climate. American Institute of Physics, pp 520

Risbey JS, Kandlikar M, Karoly DJ (2000) A framework to articulate and quantify uncertainties in climate change detection and attribution. Clim Res 16: 61–78

Roeckner E, Arpe K, Bengtsson L, Christoph M, Claussen M, Dümenil L, Esch M, Giorgetta M, Schlese U, Schulzweida U (1996a) The atmospheric general circulation model ECHAM4: model description and simulation of present-day climate. MPI Report 218, Max-Planck-Institut für Meteorologie, Hamburg, Germany, pp 90

Roeckner E, Oberhuber JM, Bacher A, Christoph M, Kirchner I (1996b) ENSO variability and atmospheric response in a global coupled atmosphere–ocean GCM. Clim Dyn 12: 737–754

Santer BD, Taylor KE, Wigley TML, Johns TC, Jones PD, Karoly DJ, Mitchell JFB, Oort AH, Penner JE, Ramaswamy V, Schwarzkopf MD, Stouffer RJ, Tett SFB (1996a) A search for human influences on the thermal structure in the atmosphere. Nature 382: 39–46

Santer BD, et al (1996b) Human effect on global climate? Nature 384: 525

Stott PA, Tett SFB (1998) Scale-dependent detection of climate change. J Clim 11: 3282–3294

Tett SFB, Johns TC, Mitchell JFB (1997) Global and regional variability in a coupled AOGCM. Clim Dyn 13: 303–323

Thomson DJ (1995) The seasons, global temperature, precession and CO_2. Science 268: 59–68

Waple AM, Mann ME, Bradley RS (2002) Long-term patterns of solar irradiance forcing in model experiments and proxy-based surface temperature reconstructions. Clim Dyn 18: 563–578

Wigley TML, Barnett TP (1990) Detection of the greenhouse effect in the observations. In: Houghton JT, Jenkins GJ, Ephraums JJ (eds) Climate Change: The IPCC Scientific Assessment. Cambridge University Press, Cambridge, UK, pp 239–256

Wigley TML, Smith RL, Santer BD (1998) Anthropogenic influence on the autocorrelation structure of hemispheric-mean temperatures. Science 282: 1676–1679